

Predissociation in the $E^1\Pi$, $v=1$ state of the six natural isotopomers of CO

W. Ubachs^{a)} and I. Velchev

Department of Physics and Astronomy, Laser Centre, Vrije Universiteit De Boelelaan 1081, 1081 HV Amsterdam, The Netherlands

P. Cacciani

Laboratoire Aimé Cotton, Campus d'Université Paris-Sud, Bât. 505, Orsay, France

(Received 16 March 2000; accepted 10 April 2000)

The $E^1\Pi$, $v=1$ state of carbon monoxide is studied in high resolution using a tunable and narrowband laser source in the vacuum ultraviolet near 105 nm. Calibration with respect to a reference standard consisting of iodine lines in the visible range, measured by saturated absorption spectroscopy, yields an absolute accuracy of 0.003 cm^{-1} for the CO resonances. Transition frequencies of the $E-X(1,0)$ band were determined for all six natural isotopomers ($^{12}\text{C}^{16}\text{O}$, $^{12}\text{C}^{17}\text{O}$, $^{12}\text{C}^{18}\text{O}$, $^{13}\text{C}^{16}\text{O}$, $^{13}\text{C}^{17}\text{O}$, and $^{13}\text{C}^{18}\text{O}$) and improved molecular constants derived. Natural lifetime broadening, caused by predissociation was investigated quantitatively for single rotational and (e)-(f) parity levels. The accidental predissociation phenomena, giving rise to line shifts and broadening, could be explained up to the experimental accuracy in a model based on spin-orbit-coupling between $E^1\Pi$, $v=1$ and $k^3\Pi$, $v=6$ states, with a coupling constant of $H_{E,k} = 1.88 \pm 0.01\text{ cm}^{-1}$ for all six isotopomers. The overall line broadening parameter Γ_E for the E state, ascribed to interaction with a repulsive $^1\Pi$ state, and Γ_k for the k state, were determined as well; the predissociation rates were found to decrease with increasing reduced mass of the isotopomers for both $E^1\Pi$, $v=1$ and $k^3\Pi$, $v=6$ states. © 2000 American Institute of Physics.

[S0021-9606(00)00726-1]

I. INTRODUCTION

The predissociation properties of the $E^1\Pi$, $v=1$ state of carbon monoxide provide, from the molecular physics perspective, an interesting case of an accidental resonance that calls for detailed spectroscopic investigations. From the astrophysics perspective this state plays an important role in the photodissociation induced isotopic fractionation in the interstellar medium. Photodissociation of CO occurs in the wavelength range 90–115 nm. An important result of medium resolution synchrotron studies¹ and subsequent rotationally resolved studies using a classical spectrograph² was that photodissociation occurs primarily through bound states of the molecule rather than via a dissociative continuum; *predissociation* is the general rule for CO. The states lying energetically above the $E^1\Pi$, $v=1$ state are known to predissociate with a yield exceeding 99%, whereas the $C^1\Sigma^+$, $v=0$ state and the states below do not at all contribute to dissociation. For the states in between, the $(3p\pi)E^1\Pi$, $v=0$ and 1, and the $(3p\sigma)C^1\Sigma^+$, $v=1$ state a competition between radiative and dissociative decay prevails with somewhat comparable rates. Since the predissociation yield will depend, more or less, on the isotopic constitution of the molecule these three vibronic levels will cause isotopic fractionation upon irradiation with vacuum ultraviolet (VUV) light. This issue was addressed in calculations of the photodecomposition and chemistry of CO in the interstellar environment, including shielding and penetration effects³ and the $E^1\Pi$,

$v=1$ state was shown to play a prominent role. Against this background we have undertaken the present study, revealing the molecular parameters governing the predissociation process for all six natural isotopomers of CO.

The VUV spectrum of CO, including the $E-X$ system, was first observed by Hopfield and Birge.⁴ Later higher resolution studies were performed^{5,6} and an accidental predissociation in the $E^1\Pi$, $v=0$ state was found.⁷ The same effect of a parity dependent predissociation, restricted to the (e)-component of the $J=31$ level, was observed in infrared Fourier-transform spectroscopy.⁸ The $E^1\Pi$ state was also observed via the $E-A$ system by Kepa (see Ref. 9 and references therein) for various isotopomers; however, only the $E^1\Pi$, $v=0$ state was observed in this emission system. The phenomenon of accidental predissociation was also observed in the $v=1$ level of the $E^1\Pi$ state, but now occurring at $J=7$ for both (e) and (f) parity levels and for both $^{12}\text{C}^{16}\text{O}$ and $^{13}\text{C}^{16}\text{O}$.^{2,10} When lasers entered the field of spectroscopy the E state of CO was reinvestigated, by double resonance excitation¹¹ and by 2+1 resonance enhanced multiphoton ionization (REMPI).¹²

The accidental predissociation in the $E^1\Pi$ state was investigated by Baker *et al.*¹³ Using 2+1 REMPI laser excitation they probed the $E-X(0,0)$ and $(1,0)$ bands for four isotopomers: $^{12}\text{C}^{16}\text{O}$, $^{13}\text{C}^{16}\text{O}$, $^{12}\text{C}^{18}\text{O}$, and $^{13}\text{C}^{18}\text{O}$. They showed that the perturbation is caused by a state of $^3\Pi$ symmetry, the same one as was previously observed, but assigned as $^3\Sigma^+$, by laser excitation combined with electron bombardment.¹⁴ After identification of the perturber state as the $k^3\Pi$ state Baker and co-workers^{15,16} used classical spec-

^{a)}Electronic mail: wimu@nat.vu.nl

trograph techniques to observe the sequence of vibrational levels. This $^3\Pi$ state had previously been observed in an electron scattering experiment resolving an irregular progression of vibrational levels.¹⁷ Before, a bound valence state of $^3\Pi$ symmetry was predicted in this energy range from *ab initio* calculations.¹⁸ Mellinger and Vidal used a double-resonance laser excitation scheme to probe two vibrational levels of the $k^3\Pi$ state.¹⁹ An important contribution to unraveling the structure of the $k^3\Pi$ perturber state was made by Berden *et al.*²⁰ They discovered that all previous studies had missed the lowest $k^3\Pi$, $v=0$ level; in a double-resonance laser experiment via the metastable $a^3\Pi$ intermediate state on $^{12}\text{C}^{16}\text{O}$ and $^{13}\text{C}^{16}\text{O}$ they showed that all measured levels had to be renumbered. The vibrational progression in the $k^3\Pi$ state is clearly perturbed near $v=5$, in the new numbering; some evidence of an interaction with the $c^3\Pi$ state was presented.²¹

In a previous paper we reported on an investigation of the $E^1\Pi$, $v=0$ and 1 states using two techniques, 2+1 REMPI and 1 VUV+1 UV photoionization.²² The spectroscopy of both states was improved and a detailed model for the spin-orbit interaction between the $E^1\Pi$ state and the $k^3\Pi$ state was presented, based on the concept introduced by Baker *et al.*¹³ Line shifts and effects on the line intensity were used to extract parameters governing the interaction for both $^{12}\text{C}^{16}\text{O}$ and $^{13}\text{C}^{16}\text{O}$. The resolution in these studies was limited to 0.3 cm^{-1} , thus limiting the accuracy of the analysis of the perturbation. Subsequently a direct lifetime measurement was performed using a picosecond VUV laser employed in a pump-probe technique.²³ By comparing the lifetimes with oscillator strengths from the literature^{2,10,24–26} values for the predissociation yield, falling in the range 80%–90%, were deduced. However, in the time-domain study no rotational resolution was obtained; the lifetimes correspond to a certain rotational distribution over the lowest J states.

The present study is another reinvestigation of the $E^1\Pi$, $v=1$ state, now with a laser system of sufficiently narrow bandwidth to unravel the predissociation effects of each separate rotational level. The laser system, tested in studies on the helium atom,²⁷ is applied to record narrow Q -branch lines of the $(4p\pi)L^1\Pi$, $v=0$ state of CO.²⁸ In this paper line broadening effects are monitored for the individual rotational lines in the $E-X(1,0)$ band that allow for a deconvolution of the natural lifetime broadening effect. The predissociation phenomenon in all six natural isotopomers is studied; moreover the high resolution laser allows for the first time an investigation of the Q -branch lines in the $E-X(1,0)$ band.

II. EXPERIMENT

The experimental setup was used before in several spectroscopic studies and described in previous publications. In short it consists of a narrowband tunable pulse-dye amplifier (PDA), seeded by the output of an argon-ion pumped continuous wave (CW) ring-dye-laser, delivering wavelength tunable pulses of 5 ns duration and 200 mJ pulse energy. These pulses are frequency doubled in a KD*P-crystal and subsequently frequency tripled in a pulsed jet of xenon gas.

Spectroscopic studies are performed on-line in a differentially pumped vacuum interaction chamber using the technique of 1 VUV+1 UV two-photon ionization. Signal is detected by monitoring the ions after mass selection in a short (25 cm) time-of-flight tube. The setup was used in a study on precision spectroscopy and lifetime measurements of the CO molecule focusing on the Q -branch lines of the $L(4p\pi)$, $v=0$ state.²⁸ All details and the experimental procedures are fully described in Refs. 27 and 28. In the following only some relevant details and changes made for the present investigation are mentioned.

For the study of the $E^1\Pi$, $v=1$ state the ring-dye laser as well the PDA system were operated on DCM dye to cover the wavelength of 630 nm. For each specific investigation a different nozzle and skimmer geometry is chosen. In the present case a skimmer of 1 mm diameter was taken, somewhat larger than in the study on He,²⁷ to achieve a higher gas density in the interaction zone. In the present study natural carbon monoxide, containing 1.1% ^{13}C , 0.2% ^{18}O and 0.03% ^{17}O was used as well as ^{13}C enriched sample (99% ^{13}C), containing about 15% ^{18}O and more than 1% ^{17}O . These two gas samples were sufficient to record spectra of all six natural isotopomers of CO. The ^{13}C -enriched sample also contained an observable amount of $^{12}\text{C}^{18}\text{O}$. Of course the signal-to-noise ratio for the spectra of $^{12}\text{C}^{17}\text{O}$ and $^{13}\text{C}^{17}\text{O}$ was not very good, because the abundance of these species in both samples was low. Special attention was given to the space-focusing conditions and the extraction voltages applied in the interaction zone; these were optimized to obtain as narrow ion signal peaks as possible, so that three gated integrators could be used for on-line registration of the VUV spectra of three different isotopes. A typical recording is displayed in Fig. 1; three spectra of CO isotopomers are recorded simultaneously with gates set at masses 29, 30, and 31. The upper three traces reflect the spectra of $^{13}\text{C}^{16}\text{O}$, $^{13}\text{C}^{17}\text{O}$, and $^{13}\text{C}^{18}\text{O}$. The ion peaks on the time-of-flight axis could not be entirely separated, particularly near the strong lines of the most abundant isotopomers, due to space charge effects occurring on the strong resonances. In Fig. 1 leaking of the strong signal of the strong $P(7)$ line of $^{13}\text{C}^{16}\text{O}$ into the time window of the heavier isotopomers is demonstrated; such artefactual spectral lines in the spectra of masses 30 and 31 are marked with a dashed vertical line. The method of simultaneous measurements helps keep the consumption of enriched gas low and the experiment affordable. During the experiment a compromise was searched between gas density, signal averaging (over five laser pulses for ^{13}C) and signal to noise. Effectively some 5 L of enriched gas was used for the entire investigation presented here.

The methods for absolute frequency calibration of the VUV resonances were described previously.^{27,28} A basic assumption is that the exact sixth harmonic of the seed frequency is generated in the chain of amplifiers and frequency converters. The saturated absorption spectrum of molecular iodine is recorded on-line using some 10 mW of the output of the cw ring-dye laser. For the previous study on the $L(4p\pi)$, $v=0$ state of CO the lines in the relevant domain (near 590 nm) were specifically calibrated in our laboratory;²⁸ the calibration procedure and the results for

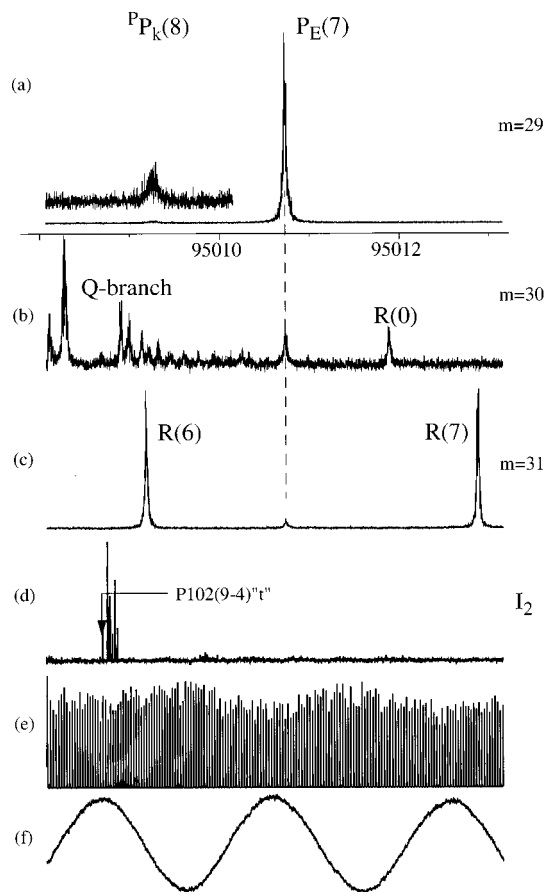


FIG. 1. Simultaneous recording of several spectra. In the upper traces the 1 VUV+1 UV photoionization spectra of CO with time of flight set at: (a) mass 29 for $^{13}\text{C}^{16}\text{O}$; (b) mass 30 for $^{13}\text{C}^{17}\text{O}$; (c) mass 31 for $^{13}\text{C}^{17}\text{O}$. The lower spectra are recorded with the cw output of the ring dye laser: (d) saturated absorption spectrum of the $P102(9-4)$ line of the $B-X$ system in iodine; (e) marker fringes of the stabilized etalon with FSR = 149.9560 MHz; (f) markers of a low finesse etalon for tracing mode hops in the scanning of the dye laser. The vertical dashed line indicates that the ghost resonances at masses 30 and 31 are in effect due to leaking of the strong signal on the $P_E(7)$ line of $^{13}\text{C}^{16}\text{O}$ into the other time windows.

more than 100 lines in the range 571–596 nm are documented in Ref. 29. In the present study reference lines near 630 nm are required. Since continuous scans are limited to 30 GHz all the saturated I_2 lines near the CO resonances had to be calibrated by similar means. In connection to this study we performed a calibration campaign determining the absolute frequency of 481 hyperfine components of I_2 transitions in the entire wavelength range of 596–655 nm with an absolute 1σ accuracy of 1 MHz. The results will be published separately.³⁰ Specifically we used the $P85$ to $P97$ and $R91$ to $R103$ lines of the $B-X(7,3)$ band and the $P92$ to $P104$ and $R90$ to $R109$ lines of the $B-X(9,4)$ band of I_2 in our frequency calibrations of the CO resonances. This range also includes the very accurately calibrated lines $P96$ and $R96$ in the $B-X(9,4)$ band by Sansonetti.³¹ The absolute frequencies of the CO resonances were determined using relative measurements in terms of frequency markers of an actively stabilized etalon with a free-spectral range (FSR) of 148.9560 ± 0.0010 MHz. A computerized procedure was used to fit the profiles of the CO resonances and the etalon

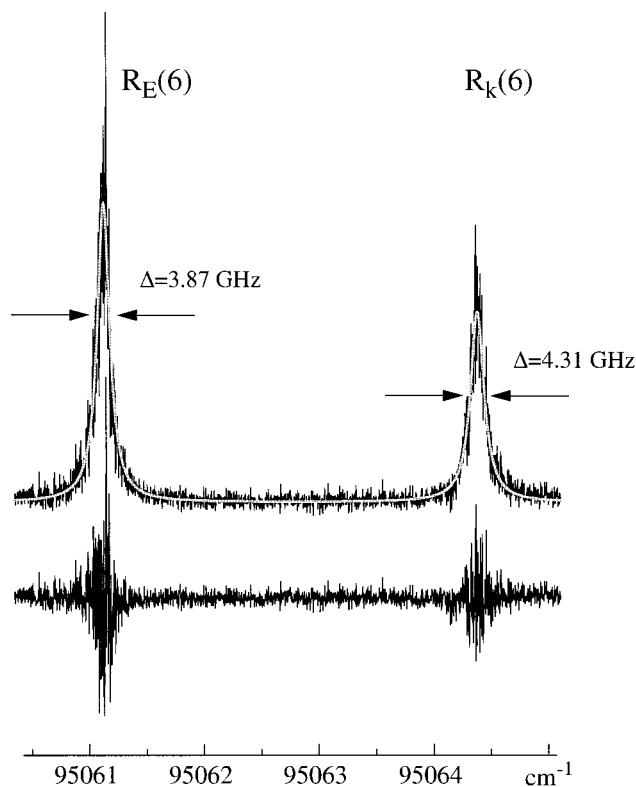


FIG. 2. Spectrum of two nearby lying resonances in $^{13}\text{C}^{16}\text{O}$. These lines represent the example of the strongest interaction between the singlet and triplet states for all isotopomers. As a result of the mixing the linewidth and intensity of both resonances are nearly equal. The lines are fitted to a Lorentzian; the result is shown as a gray-shaded line. Residuals of this fit are plotted below the recorded spectrum. The absolute frequency is determined with respect to the $R103(9,4)$ iodine line.

markers, linearize the frequency scale, and determine the separation in terms of the FSR; for the CO resonances the resulting frequency is multiplied by 6 for the harmonic generation factor. The on-line recorded I_2 -saturation spectrum, in this case of the $P102(9,4)$ line, and the etalon fringes are shown in Figs. 1(d) and 1(e) as well. Also shown in Fig. 1 is the recording of the reflection of a low finesse etalon (glass plate); such oscillatory spectra serve to detect mode hops in the scan of the ring-dye laser. The accuracy in the resulting absolute frequencies of the CO resonances is primarily determined by the relatively large bandwidth of the latter, which is associated with the predissociation phenomenon. The typical accuracy obtained for the lines with sufficient signal to noise is 0.003 cm^{-1} .

This value of 0.003 cm^{-1} does not include possible systematic effects. The issue of a nonperfect perpendicular alignment of the molecular beam with respect to the VUV and UV light beams, giving rise to a Doppler shift, was addressed. The $R(0)$ line of $^{12}\text{C}^{16}\text{O}$ and the $3p^6-3p^54s'[1/2]_1$ resonance line of argon at nearly the same wavelength were subjected to a systematic investigation; the velocity in the molecular beam was varied by using pure CO and argon samples and by mixing them with He gas, thereby increasing the average velocity in the pulsed expansion by a known amount. As a result we deduce a systematic Doppler shift of 0.001 cm^{-1} toward the blue side in the present study; the

TABLE I. Transition frequencies in the $E-X(1,0)$ band of $^{12}\text{C}^{16}\text{O}$ and deviations from a least-squares fit.

J	$R(J)$	Obs.—calc.	$Q(J)$	Obs.—calc.	$P(J)$	Obs.—calc.
0	95 086.764 ^a	-0.002				
1	95 090.670 ^a	-0.006				
2	95 094.617 ^a	-0.001				
3	95 098.588 ^a	-0.003				
4						
5	95 106.609 ^a	0.002			95 063.986 ^a	-0.004
6	95 111.020 ^a	0.005			95 060.303 ^a	0.000
7	95 114.804 ^a	0.001			95 056.635 ^a	0.000
7	95 190.051 ^{b,c}	-0.004				
8	95 118.728 ^a	-0.001	95 083.247 ^a	-0.001	95 053.364 ^a	0.004
9	95 123.423 ^a	0.003				
10	95 127.425 ^a	0.005	95 083.778 ^a	-0.003	95 045.716 ^a	0.001
11	95 131.872 ^a	-0.008	95 083.670 ^a	0.003	95 042.734 ^a	0.004
12	95 135.993 ^a	-0.001			95 039.064 ^a	0.006
13	95 140.264 ^a	0.000	95 083.991 ^a	-0.004	95 035.844 ^a	-0.005
14			95 084.113 ^a	0.002	95 032.297 ^a	-0.001
15	95 148.970 ^b	0.041	95 084.255 ^a	0.001		
16	95 153.352 ^b	0.041	95 084.415 ^a	0.003		
17	95 157.779 ^b	0.055	95 084.582 ^a	0.000	95 022.278 ^b	0.015
18	95 162.117 ^b	-0.049	95 084.765 ^a	0.003	95 018.999 ^b	0.002
19			95 084.952 ^a	-0.001	95 015.783 ^b	0.016
20			95 085.156 ^a	0.004	95 012.603 ^b	0.031
21	95 175.647 ^b	-0.018	95 085.353 ^a	-0.007	95 009.423 ^b	0.010
22	95 180.183 ^b	-0.037			95 006.232 ^b	-0.055
23	95 184.755 ^b	-0.047			95 003.163 ^b	-0.033
24	95 189.421 ^b	0.011			95 000.207 ^b	0.069
25	95 193.932 ^b	-0.112			94 997.190 ^b	0.075
26	95 198.643 ^b	-0.061			94 994.100 ^b	-0.024
27					94 991.172 ^b	0.004
28					94 988.230 ^b	-0.014

^aMeasurements with a narrowband PDA system.^bData taken with the pulsed dye laser (Ref. 22).^cObserved perturber state.TABLE II. Transition frequencies in the $E-X(1,0)$ band of $^{13}\text{C}^{16}\text{O}$ and deviations from a least-squares fit.

J	$R(J)$	Obs.—calc.	$Q(J)$	Obs.—calc.	$P(J)$	Obs.—calc.
0	95 039.647 ^a	0.001				
1	95 043.374 ^a	-0.001				
2	95 047.078 ^a	0.002			95 028.616 ^a	-0.002
3	95 050.966 ^a	-0.001			95 024.995 ^a	-0.001
4	95 054.754 ^a	0.001			95 021.380 ^b	0.033
5	95 058.507 ^a	-0.001			95 017.887 ^a	-0.001
6	95 061.121 ^a	-0.001			95 014.326 ^a	0.001
6	95 064.380 ^{a,c}	-0.009				
7	95 066.786 ^a	0.001	95 035.114 ^a	0.004	95 010.731 ^a	-0.002
8	95 070.587 ^a	0.003	95 036.657 ^a	0.001		
8					95 009.263 ^{a,c}	-0.001
9	95 074.786 ^a	0.001	95 036.592 ^a	0.000	95 004.322 ^a	0.000
10	95 078.670 ^a	-0.001	95 036.962 ^a	0.007	95 000.782 ^a	0.002
11			95 036.895 ^a	-0.001	94 997.640 ^a	-0.002
12			95 037.002 ^a	-0.003	94 994.192 ^a	0.000
13			95 037.137 ^a	-0.002	94 990.881 ^a	-0.008
14			95 037.289 ^a	-0.001	94 987.629 ^a	-0.002
15			95 037.455 ^a	-0.001	94 984.410 ^a	-0.004
16	95 103.315 ^b	-0.084	95 037.633 ^a	0.000	94 981.197 ^b	-0.039
17	95 107.473 ^b	-0.158	95 037.823 ^a	0.001	94 977.957 ^b	-0.134
18	95 111.840 ^b	-0.053	95 038.023 ^a	0.002	94 974.817 ^b	-0.164
19	95 116.070 ^b	-0.114	95 038.230 ^a	0.000	94 971.805 ^b	-0.100
20	95 120.366 ^b	-0.137	95 038.453 ^a	0.001	94 968.889 ^b	0.025
21			95 038.679 ^a	0.001		
22			95 038.916 ^a	0.000		
23			95 039.164 ^a	0.002		

^aMeasurements with the narrowband PDA system.^bData taken with the pulsed dye laser (Ref. 22).^cObserved perturber state.

TABLE III. Transition frequencies in the $E-X(1,0)$ band of $^{12}\text{C}^{18}\text{O}$ and deviations from a least-squares fit.

J	$R(J)$	Obs.–calc.	$Q(J)$	Obs.–calc.	$P(J)$	Obs.–calc.
0	92 035.495 ^a	0.000				
1	95 039.203 ^a	0.002				
2	95 043.018 ^a	–0.001			95 024.502 ^a	–0.007
3	95 046.749 ^a	–0.002			95 021.021 ^b	0.129
4	95 050.519 ^a	0.001			95 017.387 ^a	0.000
5	95 054.195 ^a	–0.003			95 013.799 ^a	0.001
6	95 059.244 ^b	0.028			95 010.235 ^a	–0.008
7	95 062.493 ^a	0.001			95 006.537 ^b	–0.068
8	95 066.280 ^a	–0.001	95 032.475 ^a	0.001	95 004.278 ^b	–0.027
9	95 070.438 ^a	–0.001	95 032.427 ^a	0.002	95 000.350 ^b	0.084
10	95 074.385 ^b	0.018			94 996.889 ^b	0.147
11	95 078.364 ^b	–0.023	95 032.742 ^a	–0.009	94 993.665 ^b	0.075
12			95 032.872 ^a	0.006	94 990.175 ^b	–0.035
13			95 033.006 ^a	0.000	94 987.073 ^b	0.148

^aMeasurements with the narrowband PDA system.^bData taken with the pulsed dye laser (Ref. 22).

resonances were corrected for this shift (see also Ref. 32). As discussed in Ref. 27 frequency chirp in the dye amplifier will also result in a net shift of the deduced center frequency of the spectral resonances; we did not address this issue in the present study. The absolute line positions may be shifted due to this chirp phenomenon by an amount which is estimated to be less than 0.003 cm^{-1} ; however, the frequency separations will not be affected by this phenomenon.

The recorded spectral profiles were fitted to Lorentzian profiles to derive information on the intrinsic molecular line broadening associated with predissociation. In Fig. 2 observed spectra of two nearby lying lines are shown with the fitted Lorentzians and the residuals of the fitting procedure. The frequency scale is derived from interpolation with the markers of the stabilized etalon. The residuals show that there is no systematic deviation from Lorentzian profiles. This statement holds for the relatively broad ($>1\text{ GHz}$) resonances, where natural lifetime broadening associated with predissociation is the dominant effect, but also for the narrowest resonances observed for $^{13}\text{C}^{18}\text{O}$ (650 MHz) a Lorentzian profile is still a good approximation. The instrument width in the experimental setup is a combined effect of the laser linewidth (after harmonic conversion) and Doppler effects related to divergence of the VUV beam and the molecular beam. Effects on the linewidth of the strong $R(0)$ line of $^{12}\text{C}^{16}\text{O}$ under varying geometrical conditions and gas densities were systematically studied. Collisional effects are absent in the skimmed molecular beam expansion with the interaction zone 30 nozzle diameters (0.8 mm) away from the beam source. In the chosen geometrical configuration with a nozzle-skimmer distance of 6 cm and a skimmer diameter of 1 mm the laser linewidth is the dominant contribution to the instrument width. The natural line broadening can be deconvoluted from the observed widths by taking the instrument function as a Lorentzian of 300 MHz. This was tested also in an investigation of the $3p^6-3p^54s'[1/2]_1$ resonance line of argon in the same configuration and at the same wave length of 105 nm.³² In that case the linewidth was found to be about 450 MHz including the contribution of the Doppler effect. It should be understood that a Gaussian com-

ponent (of about 150–200 MHz) related to a Doppler effect does only play a minor role in the deconvolution procedure of broad lines; effectively only the Lorentzian contribution is of importance. Hence the natural line broadening effect was deduced via: $\Gamma = \Delta_{\text{obs}} - \Delta_{\text{instr}}$ with $\Delta_{\text{instr}} = 300\text{ MHz}$. This procedure is certainly valid for the lines exceeding widths of 1 GHz; for the narrower lines the procedure is less accurate.

III. RESULTS AND ANALYSIS

A. Spectroscopy

The spectral data on the observed $E-X(1,0)$ bands are presented as listings of frequency positions in Tables I–VI

TABLE IV. Transition frequencies in the $E-X(1,0)$ band of $^{13}\text{C}^{18}\text{O}$ and deviations from a least-squares fit. All measurements were taken with the narrowband PDA system.

J	$R(J)$	Obs.–calc.	$Q(J)$	Obs.–calc.
0	94 988.815 ^a	–0.005		
0	94 985.052	0.000		
1	94 991.596	0.001	94 985.321 ^b	–0.003
2	94 994.787	0.001	94 984.567	0.004
3	94 998.226	0.001	94 984.205 ^b	0.004
4	95 001.770	0.000	94 984.069	–0.001
5	95 005.189	0.000	94 984.029	0.000
6	95 009.176	–0.001	94 983.889	0.000
7	95 012.871	0.000	94 984.205 ^b	–0.007
8	95 016.629	0.008	94 984.263	0.001
9			94 984.350	–0.003
10	95 024.231	0.000	94 984.465	0.000
11	95 028.082	–0.003	94 984.595	0.002
12			94 984.736	0.000
13	95 035.885	0.001	94 984.894	0.001
14	95 039.828	0.000	94 985.060	–0.002
15	95 043.799	–0.001	94 985.245 ^b	0.001
16	95 047.802	0.001	94 985.437	0.000
17	95 051.831	0.001	94 985.646	0.003
18	95 055.886	0.001	94 985.857	–0.003
19	95 059.967	–0.001		
20	95 064.077	0.000		

^aObserved perturber state.^bBlended lines (partially).

TABLE V. Transition frequencies in the $E-X(1,0)$ band of $^{12}\text{C}^{17}\text{O}$ and deviations from a least-squares fit. All measurements were taken with the narrowband PDA system. The Q -branch lines were observed in a cold beam populating only the lowest J levels.

J	$R(J)$	Obs. - calc.	$Q(J)$	Obs. - calc.
0	95 059.735	-0.008		
1	95 063.543	0.003	95 055.991	0.014
2			95 055.991	0.001

for the six natural isotopomers of CO. The accuracy of the well-resolved rotational lines with sufficient signal to noise is 0.003 cm^{-1} . It is noted that this does not include the additional uncertainty in the absolute frequency due to frequency chirp in the dye amplifiers; a systematic shift of the entire set of spectral data of up to 0.003 cm^{-1} is possible. The identification of R and P -branch lines, probing (e)-parity states, is straightforward since these lines follow a progression, even in cases of strong perturbations; there is no case where the order in the rotational progression is reversed. The example of the strongest perturbative effect, near $J=7$ in the $^{13}\text{C}^{16}\text{O}$ isotopomer, probed via the R -branch, is displayed in Fig. 2.

The assignment of Q -branch lines is more difficult because small perturbations give rise to reshuffling of the order of the rotational lines. Also the information on the (f)-parity components available from previous studies is less accurate, since the Q -branch lines could not be resolved in one-photon $E-X(1,0)$ bands, while in two-photon excitation the R and P transitions probing (f) components are sometimes overlapped with O and S transitions. For this reason we focus on the Q branches in the presentation of the data. In Figs. 3–8 spectral recordings with assignments are shown for the Q branches of the six natural isotopomers of CO. It is for the first time that these spectral structures are resolved; the width of the lines is primarily determined by the natural lifetime broadening effect associated with predissociation. The assignment of Q -branch lines was performed after a full analysis of the more easily resolved (e)-parity states. In principle the rotational structure of the excited states is described separately for the (e) and (f) parity component.

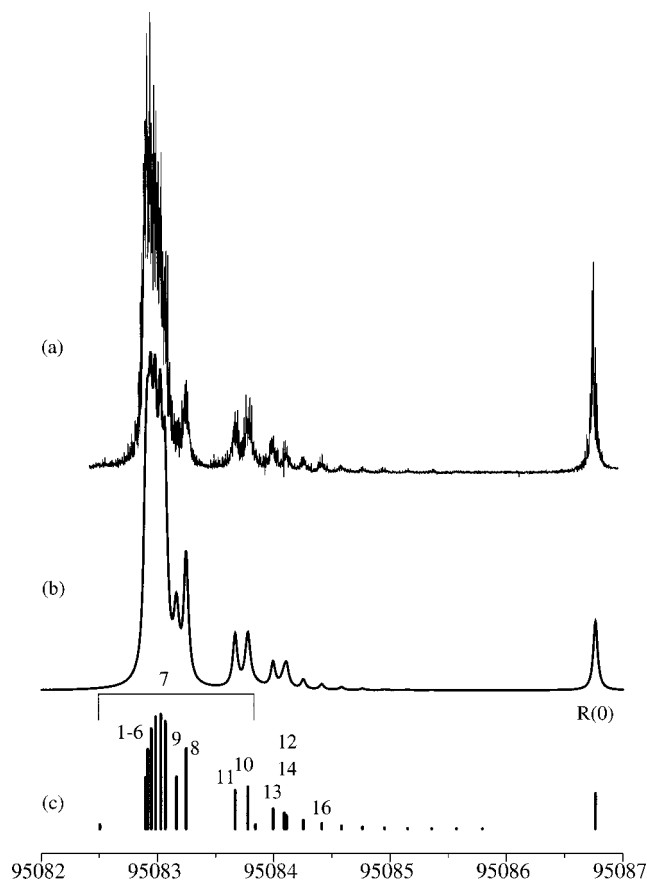


FIG. 3. Q branch of $^{12}\text{C}^{16}\text{O}$: (a) recorded spectrum with 1 VUV+1 UV photoionization; (b) reconstructed spectrum based on calculated line positions, intensities, and widths (including the effect of predissociation); (c) calculated stick spectrum representing positions and intensities. The rotational temperature is assumed to be 140 K.

In the analysis of the rotational structure the energy levels of the ground state are expressed with

$$E_X(J) = B_X J(J+1) - D_X J^2(J+1)^2 + H_X J^3(J+1)^3,$$

where the ground state molecular constants B_X , D_X , and H_X are obtained from the accurate infrared work of Guelachvili *et al.*³³ They have determined the rotational structure for seven isotopomers, including $^{14}\text{C}^{16}\text{O}$ and the six natural

TABLE VI. Transition frequencies in the $E-X(1,0)$ band of $^{13}\text{C}^{17}\text{O}$ and deviations from a least-squares fit. All measurements were taken with narrowband PDA system.

J	$R(J)$	Obs. - calc.	$Q(J)$	Obs. - calc.	$P(J)$	Obs. - calc.
0	95 011.883	-0.001				
1	95 015.506	0.008	95 008.283	-0.001		
2	95 019.110	0.002	95 008.283	0.000		
3	95 022.596	0.000	95 008.250	-0.007	94 997.601	-0.004
4			95 008.099	-0.003		
5			95 009.970	0.002		
6	95 034.492	0.000	95 008.987	-0.004		
7			95 008.900	-0.001		
8	95 042.206	-0.001	95 008.685	0.000		
9			95 009.131	0.001		
10			95 009.207	0.004		
11			95 009.316	-0.001		
12	95 057.874	-0.000	95 009.451	0.001		

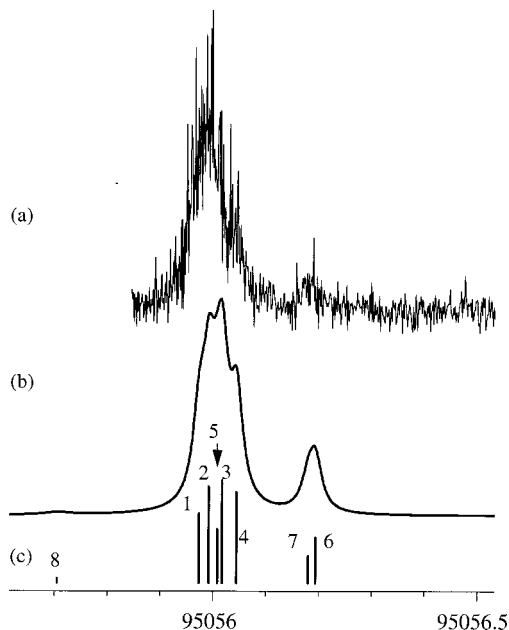


FIG. 4. Q branch of $^{12}\text{C}^{17}\text{O}$ and a calculated spectrum with $T_{\text{rot}}=60$ K.

ones, with a very high accuracy. From the Dunham parameters listed in Ref. 33 we have derived values for B_X , D_X , and H_X ; the values are listed in Table VII. The energy level structure for the $E^1\Pi$, $v=1$ excited state is in first order expressed as

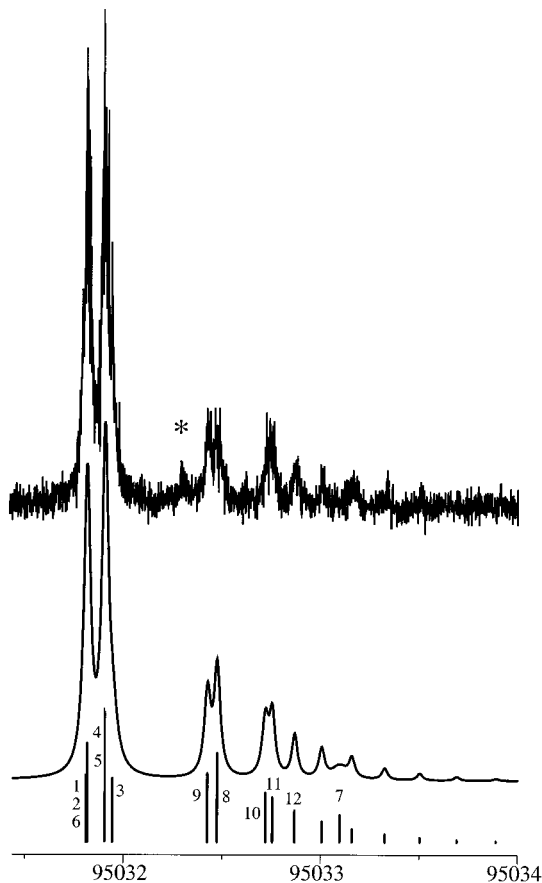


FIG. 5. Q branch of $^{12}\text{C}^{18}\text{O}$ and a calculated spectrum with $T_{\text{rot}}=140$ K. The resonance indicated with (*) pertains to the $^{12}\text{C}^{16}\text{O}$ isotopomer.

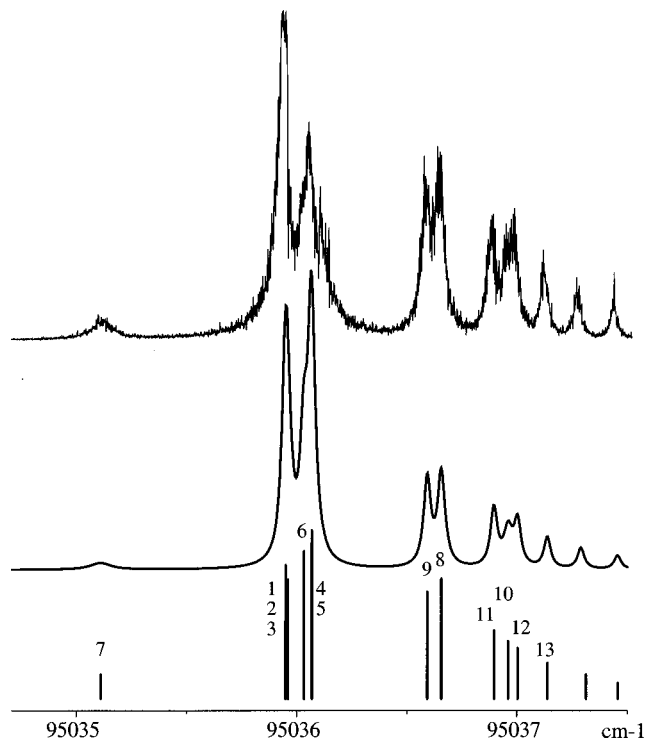


FIG. 6. Q branch of $^{13}\text{C}^{16}\text{O}$ and a calculated spectrum with $T_{\text{rot}}=160$ K. The $Q(7)$ line, shifted by a large amount, is clearly visible.

$$E_E^{e,f}(J) = \nu_E + B_E^{e,f}J(J+1) - D_E^{e,f}J^2(J+1)^2,$$

where the rotational constants B and D are taken for (e) and (f) parity components separately. We have assumed a single value for the band origin ν_E for both parities. As discussed previously^{13,22} the rotational energy levels of the $E^1\Pi$, $v=1$ excited state are perturbed by the $k^3\Pi$ state; since the work of Berden *et al.*²⁰ we know that it is the $v=6$ vibrational level which causes the interaction. The $k^3\Pi$ state is represented in matrix form k_{ij} on the basis ($^3\Pi_2$, $^3\Pi_1$, $^3\Pi_0$) by³⁴⁻³⁶

$$k_{11}(J) = \nu_k + A_{LS} + B_k(x-3) - D_k(x^2 - 4x + 5),$$

$$k_{12}(J) = k_{21}(J) = -[B_k - 2D_k(x-1)]\sqrt{2(x-2)},$$

$$k_{22}(J) = \nu_k + B_k(x+1) - D_k(x^2 + 6x - 3),$$

$$k_{23}(J) = k_{32}(J) = -[B_k - 2D_k(x+1)]\sqrt{2x},$$

$$k_{13}(J) = k_{31}(J) = -2D_k\sqrt{x(x-2)},$$

$$k_{33}(J) = \nu_k - A_{LS} + B_k(x+1) - D_k(x^2 + 4x + 1) \mp C_k,$$

with $x = J(J+1)$ and where the $(-)$ sign in the last equation is for the (e) parity levels and the $(+)$ sign for the (f) parity levels. Hence the C_k constant represents the effect of Λ doubling in the triplet state. Since the $k^3\Pi$ state is only observed indirectly some small higher order matrix elements have been neglected. The energy levels of the $E^1\Pi$, $v=1$ state, and in the $k^3\Pi$, $v=6$ state, in the perturbed situation follow after diagonalization of the matrix:

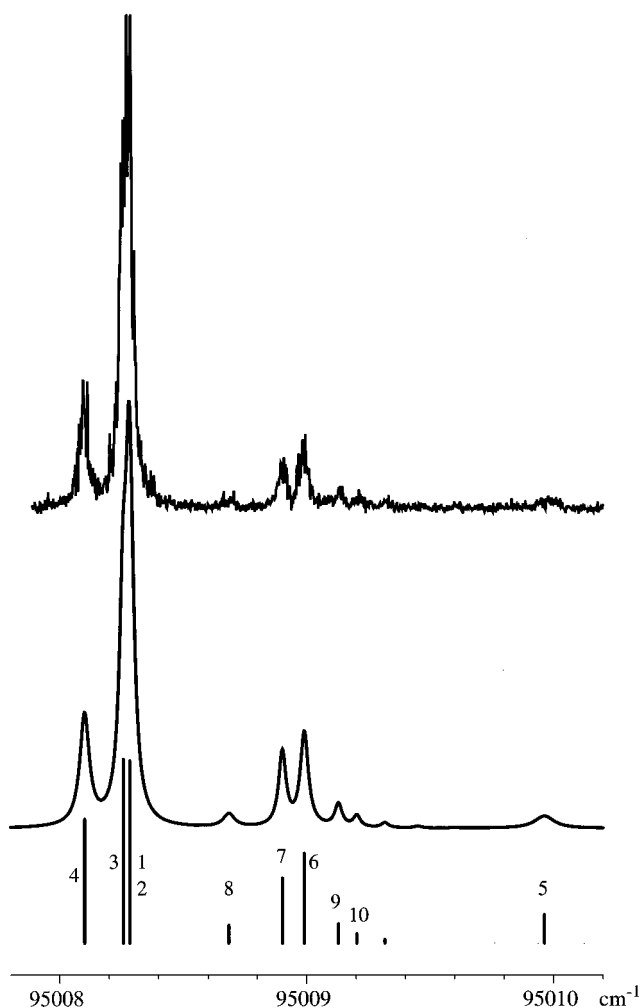


FIG. 7. Q branch of $^{13}\text{C}^{17}\text{O}$ and a calculated spectrum. The $Q(5)$ line is most strongly perturbed in this case.

$$M(J) = \begin{bmatrix} E_E^{e,f}(J) & 0 & H_{E,k} & 0 \\ 0 & k_{11}(J) & k_{12}(J) & k_{13}(J) \\ H_{E,k} & k_{21}(J) & k_{22}(J) & k_{23}(J) \\ 0 & k_{31}(J) & k_{32}(J) & k_{33}^{e,f}(J) \end{bmatrix}$$

for each value of J and for (e) and (f) parity components separately. In the present work we will consider the spin-orbit interaction matrix element $H_{E,k}$, coupling the $E^1\Pi$, $v=1$ state to the $^3\Pi_1$ component of the k state, as a fitting parameter. Some aspects of the physical origin are discussed in Ref. 22. Here it is a J -independent coupling parameter. Since the matrix $M(J)$ is not diagonal also the $\Omega=0$ and 2 components, on a Hund's case (a) basis, are affected by the perturbation and, in turn, perturb the $E^1\Pi$ state. As was shown in Ref. 22, the structure of the matrix with the appropriate constants is such that at very low J values the Hund's case (a) representation is a good approximation, but near $J=15$ there is a transition to Hund's case (b); for all J the $^3\Pi_2$ and $^3\Pi_0$ components have some $^3\Pi_1$ character coupling to the E state.

The matrix $M(J)$, with all implicit molecular constants, is included in a least-squares fitting routine, in which the transition frequencies of P , Q , and R lines are calculated

from the eigenvalues of the matrix for both parities and the ground state energies. Eigenvalues with dominant E -state character are assigned as E -state levels. Several ingredients are used to find optimum convergence in the description of the data. Based on an initial fit on the (e) components a calculation of the (f) components is performed by keeping the interaction constant $H_{E,k}$ at the same value; throughout the paper $H_{E,k}$ was considered independent of the parity. Also the trend that B_E^e is some 0.6% larger than B_E^f is considered; as discussed by Baker *et al.*¹³ the (e) levels are shifted upward in energy due to an interaction with the $C^1\Sigma^+$ state, a phenomenon of l -uncoupling in a $3p\sigma-3p\pi$ Rydberg complex. Then the Q -branch lines could be readily assigned, except for the ones at a crossing point with one of the three spin-orbit components of the $k^3\Pi$ state. Input on the $k^3\Pi$ state is required to find a proper assignment and a model for the perturbed regions. If the starting values for the $k^3\Pi$ parameters are chosen such that the triplet and singlet levels are in the wrong order convergence will generally not be found, because perturbing energy shifts are very sensitive to the initial values. For the $^{12}\text{C}^{16}\text{O}$ isotopomer the energy levels of the $k^3\Pi$ perturber are constrained by including 16 lines in the $k-X(6,0)$ band observed by Baker and co-workers^{13,15} and the $^QQ(1)$ and $^RR(1)$ lines observed by Berden *et al.*²⁰ Also the perturbed line with dominant triplet-character in Ref. 22 was included. In the final least-squares fit all data, the ones presently measured by the PDA system, the ones measured previously by 1+1 and by 2+1 REMPI,²² and the ones pertaining to the $k-X(6,0)$ band were taken as the input set in a simultaneous optimization. These data were weighted with the uncertainties as reported. For the $^{12}\text{C}^{16}\text{O}$ isotopomer the 11 parameters for the $E^1\Pi$, $v=1$ and $k^3\Pi$, $v=6$ states and the interaction matrix element were all varied resulting in the values listed in Table VII; in fact a 12th parameter was included allowing for a systematic shift of the 2+1 REMPI data.²² For the $^{13}\text{C}^{16}\text{O}$ isotopomer the five lines of Berden *et al.*²⁰ were included as well as the accurately determined frequencies of the $^PP(8)$ line (see Fig. 1) and $^RR(6)$ line (see Fig. 2). For $^{13}\text{C}^{16}\text{O}$ also a large number of frequencies from 1+1 and 2+1 REMPI spectra²² were available and included. For all other isotopomers the information on the $E^1\Pi$, $v=1$ state is less abundant. Only for $^{13}\text{C}^{18}\text{O}$ a single perturber line was found, the $^RR(0)$ line.

For a proper modeling of the singlet-triplet perturbation, and in view of the sensitivity on the input parameters for the perturber, the molecular constants for $k^3\Pi$, $v=6$ of the less abundant species were calculated by isotopic scaling. Molecular parameters were derived via

$$T_v = T_e + \omega_e(v + \frac{1}{2}) + \omega_e x_e(v + \frac{1}{2})^2,$$

$$B_v = B_e - \alpha_e(v + \frac{1}{2}),$$

where all available information on the various v levels^{13-15,19,20} was included. The spectroscopic constants for the $k^3\Pi$, $v=6$ level of $^{12}\text{C}^{17}\text{O}$, $^{12}\text{C}^{18}\text{O}$, $^{13}\text{C}^{17}\text{O}$, and $^{13}\text{C}^{18}\text{O}$ were then derived via

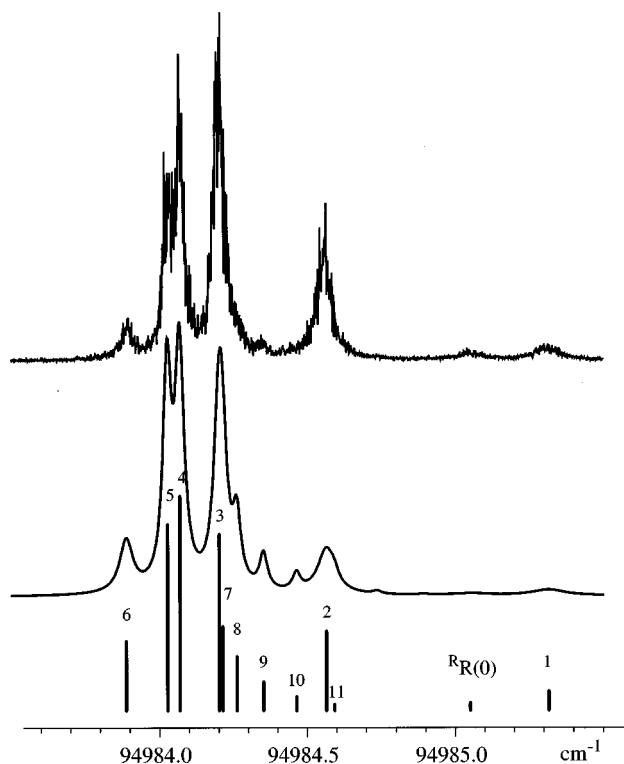


FIG. 8. Q branch of $^{13}\text{C}^{18}\text{O}$ and a calculated spectrum with $T_{\text{rot}}=60$ K. In this case the perturbation occurs at the lowest J values. This is reflected in the large shift of the $Q(1)$ line and the clearly observable transition to the state with dominant triplet character $^R R(0)$.

$$T_e^i = T_e, \quad \omega_e^i = \omega_e \rho, \quad \omega_e x_e^i = \omega_e x_e \rho^2,$$

$$B_e^i = B_e \rho^2, \quad \alpha_e^i = \alpha_e \rho^3,$$

where the indexed constants can be calculated with respect to $^{12}\text{C}^{16}\text{O}$ or $^{13}\text{C}^{16}\text{O}$ and $\rho = \sqrt{\mu/\mu_i}$ with μ and μ_i the reduced masses of the isotopomers.

In several cases, where the spectral information was scarce, the parameters for the $k^3\Pi$, $v=6$ state were kept constant at the values obtained from the isotopic scaling analysis. For $^{12}\text{C}^{17}\text{O}$ and $^{12}\text{C}^{18}\text{O}$ even the band origin was kept fixed, while for the fits pertaining to $^{13}\text{C}^{17}\text{O}$ and $^{13}\text{C}^{18}\text{O}$ the band origin was slightly varied in order to optimize the description of the interaction. In Table VII all resulting constants for the six isotopomers are listed; the parameters kept fixed in the fitting routines are indicated.

The fitting procedure for $^{13}\text{C}^{18}\text{O}$ represents an exemplary case for the problems encountered. Convergence can be found with reversed identification of $R(0)$ and $^R R(0)$ lines and change of assignment of $Q(1)$ into $^Q Q(1)$; then the $R(0)$ line is off by 0.04 cm^{-1} only with an interaction parameter converging to $H_{E,k} = 2.02 \text{ cm}^{-1}$. With the identification of Table IV a reduction of the χ^2 -value by a factor of 5 is established and a value $H_{E,k} = 1.86 \text{ cm}^{-1}$ results, more in accordance with the other isotopomers. This minimum in χ^2 was not easy to find because of the near degeneracy of the band origins of the E and k states in $^{13}\text{C}^{18}\text{O}$; the deperturbed values differ by only 0.5 cm^{-1} . At the lowest rotational level ($J=1$) the two (e) components mix in a fraction 58%/42% (absolute squares of the eigen vectors) on a pure ($^1\Pi, ^3\Pi_1$) basis. With a slight variation of the parameters the dominant $^1\Pi$ character easily swaps from one line to the other, thereby frustrating the minimization procedure. It is only by virtue of the high accuracy obtained in the present data that the interaction in $^{13}\text{C}^{18}\text{O}$ could be modeled properly. In the $^{13}\text{C}^{16}\text{O}$ isotopomer the mixing fraction at $J=7(e)$ is even 53%/47%. In the latter case the shifts of the energy levels at $J=7$, due to the interaction is 1.544 cm^{-1} for the (e) component and 1.254 cm^{-1} for the (f) component.

The fitting routines are essential in finding the proper identification of the resonances, particularly in the Q branches. In Fig. 3 the Q branch of the $^{12}\text{C}^{16}\text{O}$ isotopomer is displayed. The $Q(1)$ – $Q(6)$ are piled up in a single broad

TABLE VII. Molecular constants for the various CO isotopomers of the $E^1\Pi$, $v=1$ state and the perturbing $k^3\Pi$, $v=6$ state as derived in the present work. For convenience also the constants for the ground state are given as deduced from the work of Guelachvili *et al.* (Ref. 33). All values are in cm^{-1} .

	$^{12}\text{C}^{16}\text{O}$	$^{12}\text{C}^{17}\text{O}$	$^{12}\text{C}^{18}\text{O}$	$^{13}\text{C}^{16}\text{O}$	$^{13}\text{C}^{17}\text{O}$	$^{13}\text{C}^{18}\text{O}$
$X^1\Sigma_g^+$						
B_0	1.922 529	1.873 963	1.830 981	1.837 972	1.789 397	1.746 408
D_0	6.1203×10^{-6}	5.814×10^{-6}	5.5300×10^{-6}	5.5926×10^{-6}	5.3002×10^{-6}	5.0480×10^{-6}
H_0	5.4794×10^{-12}	5.074×10^{-12}	4.733×10^{-12}	4.768×10^{-12}	4.418×10^{-12}	4.107×10^{-12}
$E^1\Pi$, $v=1$						
v_1	95 026.9348	95 056.019	95 031.897	95 036.026	95 008.452	94 983.712
B_e	1.939 39	1.890 ^a	1.847 05	1.854 34	1.805 47	1.762 26
B_f	1.927 99	1.8795	1.836 877	1.843 95	1.795 59	1.752 86
D_e	6.67×10^{-6}	6.0×10^{-6} a	4.54×10^{-6}	6.0×10^{-6}	5.7×10^{-6}	5.66×10^{-6}
D_f	6.64×10^{-6}	6.0×10^{-6} a	5.13×10^{-6}	6.2×10^{-6}	5.7×10^{-6}	5.64×10^{-6}
$k^3\Pi$, $v=6$						
v_6	95 159.36	95 113.1 ^a	95 070.0 ^a	95 076.95	95 027.99	94 983.25
B	1.164	1.13 ^a	1.11 ^a	1.11 ^a	1.08 ^a	1.07
D	1.63×10^{-5}	1.1×10^{-5} a	1.0×10^{-5} a	1.0×10^{-5} a	1.0×10^{-5} a	1.0×10^{-5} a
A	30.21	30.0 ^a	30.9 ^a	30.5	31.4	30.53
c	0.47	0.4 ^a	0.41 ^a	0.44 ^a	0.4 ^a	0.4 ^a
H_{int}	1.892	1.88 ^a	1.884	1.885	1.88 ^a	1.864

^aValue kept constant in fitting routine.

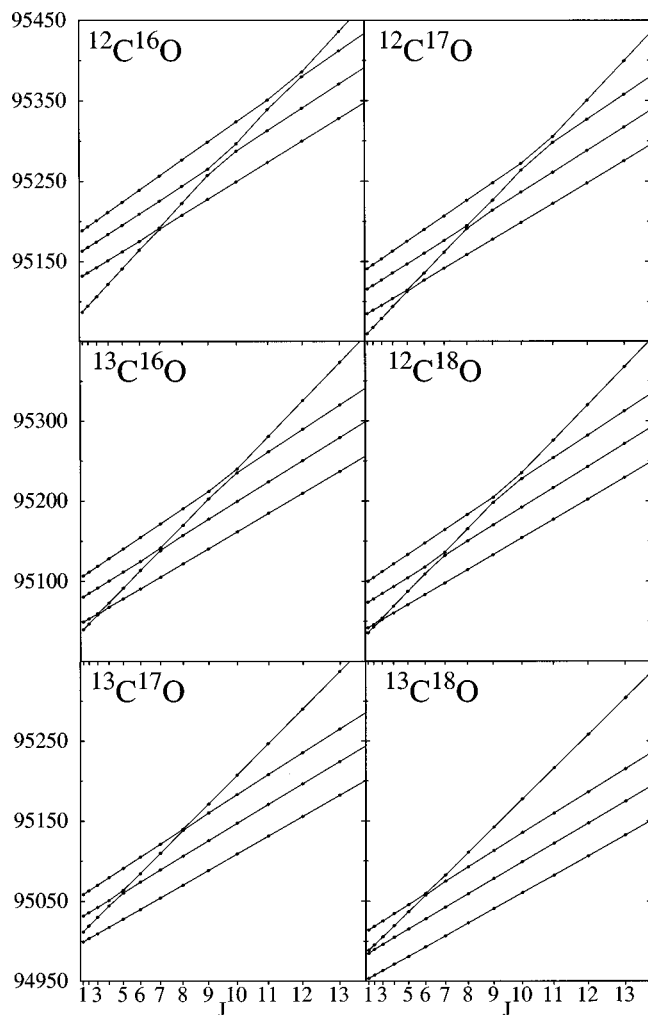


FIG. 9. Energy levels of the $E^1\Pi, v=1$ and $k^3\Pi, v=6$ states as a function of J for the various isotopomers of CO. Levels are calculated from the molecular constants given in Table VII. On the level of accuracy of this plot differences between (e) and (f) parity are not visible. The singlet-triplet interaction occurs at different values of J for each isotopomer.

resonance as indicated by the stick spectrum representing the calculated positions. As a result of the perturbations the $Q(7)$ line is shifted and broadened. Also the order of the $Q(8)$ and $Q(9)$ lines is reversed due to the interaction with the $^3\Pi_1$ component of the $k^3\Pi, v=6$ state. The same holds for the $Q(10)$ and $Q(11)$ lines. The $Q(12)$ line is strongly shifted due to interaction with the $^3\Pi_1$ component. Apart from a stick spectra calculated spectra are displayed as well in Figs. 3–8(b), where the linewidths (J dependent; see the following) are taken into account. Also the reduction of line intensity as a result of the competition between predissociation and ionization in a resonance enhanced two-photon ionization experiment is accounted for in these calculated spectra; the quantitative treatment of intensity loss in a two-photon ionization study caused by predissociation was explained in a previous paper.²² For the calculated spectrum one additional parameter was adjusted to produce a good match with the observed spectrum; the rotational temperature in the molecular beam. Not in all recorded spectra is the temperature the same since it can be manipulated somewhat

by choosing different conditions in the molecular beam expansion.

In Fig. 4 the Q branch of the $^{12}\text{C}^{17}\text{O}$ isotopomer shows only two weak and broad features, as a result of the low abundance of this species in the molecular beam. The main feature is the resulting pile of lines $Q(1)$ – $Q(5)$ in the bandhead, while the shifted $Q(6)$ and $Q(7)$ lines produce the second very weak feature as indicated. The strongly perturbed $Q(8)$ line could not be observed, due to low population of $J=8$ in the beam and the intensity loss resulting from predissociation. Figure 5 shows a recorded Q branch for $^{12}\text{C}^{18}\text{O}$. Here two prominent interactions occur at $J=7$ and $J=9$. The $J=7$ level interacts strongly with the $^3\Pi_1$ component giving rise to a shift of the $Q(7)$ line to the position of $Q(14)$. The broadened line at 95033.2 cm^{-1} gives an indication of the $Q(7)$ line, which is weakened by predissociation. The interaction with the $^3\Pi_2$ component causes the reversing of the order of $Q(8)$ and $Q(9)$ and of the shift of the $Q(10)$ lines. The perturbation at low J values, due to the $^3\Pi_0$ component, causes the shift of the $Q(3)$ line and the gap in the bandhead region. The $Q(6)$ line is shifted toward lower energy, due to interaction with $^3\Pi_1$, and coincides with $Q(1)$ and $Q(2)$.

Since the reduced mass of $^{13}\text{C}^{16}\text{O}$ does not deviate much from that of $^{12}\text{C}^{18}\text{O}$ the interactions take place at similar J values; again the strongest effect occurs at $J=7$. But in the case of $^{13}\text{C}^{16}\text{O}$ the $J=7$ level with dominant E -state character is shifted toward lower energy. As a result of good signal-to-noise ratio $Q(7)$ is well visible as a broadened feature. The perturbation of the $J=7$ level of the $^{13}\text{C}^{16}\text{O}$ isotopomer is the strongest of all for the interaction between the $E^1\Pi, v=1$ and $k^3\Pi, v=6$ states. The perturber component of dominant k -state character is observed as the $Q(7)$ line at 95038.5 cm^{-1} , where it overlaps with the $Q(20)$ line. Again the gap in the bandhead region occurs in the same way as well as the reversing of the order of $Q(8)$ and $Q(9)$ lines. The $Q(10)$ line is shifted somewhat further, so that it falls in between $Q(11)$ and $Q(12)$, giving rise to a broadened structure comprising $Q(10)$ and $Q(12)$ lines.

For the heavier $^{13}\text{C}^{17}\text{O}$ isotopomer the perturbations are further shifted toward lower J values. The strong interaction with the $^3\Pi_1$ component now occurs at $J=5$. The $Q(5)$ line is broadened and shifted away from the other Q lines toward higher energies, while the $Q(4)$ line is shifted to the red side of the Q bandhead lines. Also the $Q(6)$ line is affected; it is shifted to higher energies exhibiting a reversal with the $Q(7)$ line. The interaction with the $^3\Pi_2$ component occurs at $J=8$; the $Q(8)$ line loses intensity and is shifted to the red. The $^{13}\text{C}^{17}\text{O}$ isotopomer is the first one heavy enough so that the $^3\Pi_0$ component does not cross with the $E, v=1$ state, as shown in Fig. 9.

For $^{13}\text{C}^{18}\text{O}$ the situation is reached that the $^3\Pi_1$ component interacts with the lowest J value in $E^1\Pi, v=1$. The $J=1$ levels are shifted toward higher energy, for both (e) and (f) components. Indeed the $Q(1)$ line is largely broadened, due to predissociation and shifted away from all other Q -branch lines. The (e) parity component of $E^1\Pi, v=1, J=1$, observed in the R branch, is also shifted upward in energy; its interaction partner, the $k^3\Pi, v=6, J=1$ (e) level

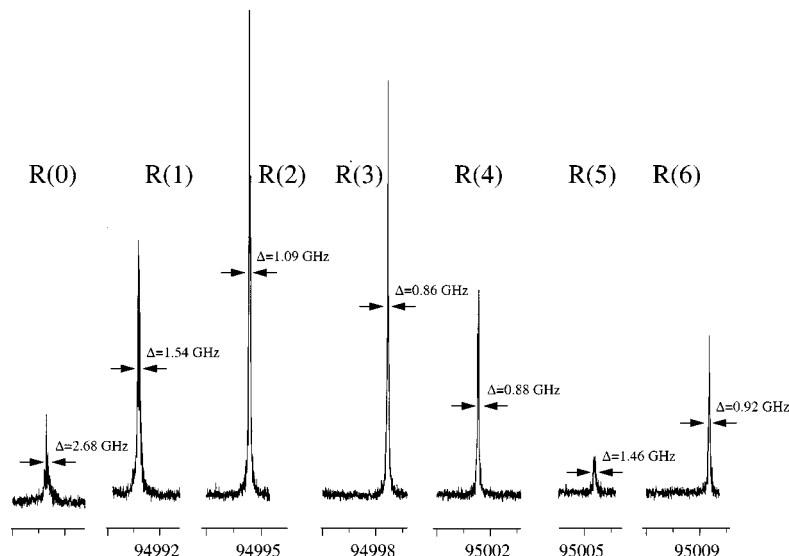


FIG. 10. Individual recording of the R -branch lines for the $^{13}\text{C}^{18}\text{O}$ isotopomer all on the same intensity scale. Linewidths are indicated.

is shifted toward lower energy by the same amount and becomes visible as a largely broadened feature indicated with R^0 in Fig. 8. In this case of $^{13}\text{C}^{18}\text{O}$ all low J values are affected by the interaction with the $^3\Pi_1$ component; all levels in the sequence $J=2-5$ are in reversed order, while $J=6$ is the first to be affected by the $^3\Pi_2$ component and undergoes a downward shift.

The location of the accidental perturbations is illustrated in the plot of the energy levels versus the rotational quantum numbers for all six isotopomers in Fig. 9. The calculated energy levels of both the $E^1\Pi$, $v=1$ and $k^3\Pi$, $v=6$ states are displayed, where an average is taken over (e) and (f) parity components; on the scale of Fig. 9 differences between the parity components are not visible. Due to the isotope-dependent vibrational level spacings, the interactions occur at lower rotational levels for the species of higher reduced mass; this effect is clearly visible in the figure.

The transition frequencies, listed in Tables I–VI for the six isotopomers are well represented by the model of the interaction between the $^1\Pi$ and $^3\Pi$ states. The resulting parameters of Table VII represent the data within the expected uncertainties of 0.003 cm^{-1} . The deviations from the fits are in fact below this value, indicating that indeed a precision of 0.003 cm^{-1} is reached. In the case of the largest perturbation, the $J=7$ level for the $^{13}\text{C}^{16}\text{O}$ isotopomer, reaching shifts of 1.5 cm^{-1} , the interaction model represents the energy levels up to an accuracy of a few 0.001 cm^{-1} , even though only a single interaction parameter is invoked.

B. Predissociation

Information on the predissociation behavior in the $E^1\Pi$, $v=1$ state can be deduced for each singly resolved rotational quantum level and for both (e) and (f) parities independently. All resolved spectral lines were fitted to Lorentzian line shapes and the linewidths were determined. In Fig. 2 a comparison between the recorded spectrum and the fitted Lorentzian is made by explicitly showing the residuals from the fit to the line shape. In that case no systematic deviations from a Lorentzian are found; only the residuals are larger

close to line center as a result of the increased intensity noise. Also in cases where the lines are narrower, particularly for the lines of $^{13}\text{C}^{18}\text{O}$, a Lorentzian function still well reproduces the observed line shapes. In Fig. 10 the seven lowest rotational lines of the R branch of $^{13}\text{C}^{18}\text{O}$ are displayed on the same intensity scale with the linewidths displayed. The effect of the interaction with the $k^3\Pi$, $v=6$ state is threefold: in addition to the line shifts at low J as discussed previously, the resonances are broadened and of decreased intensity for those levels that strongly interact with the triplet state.

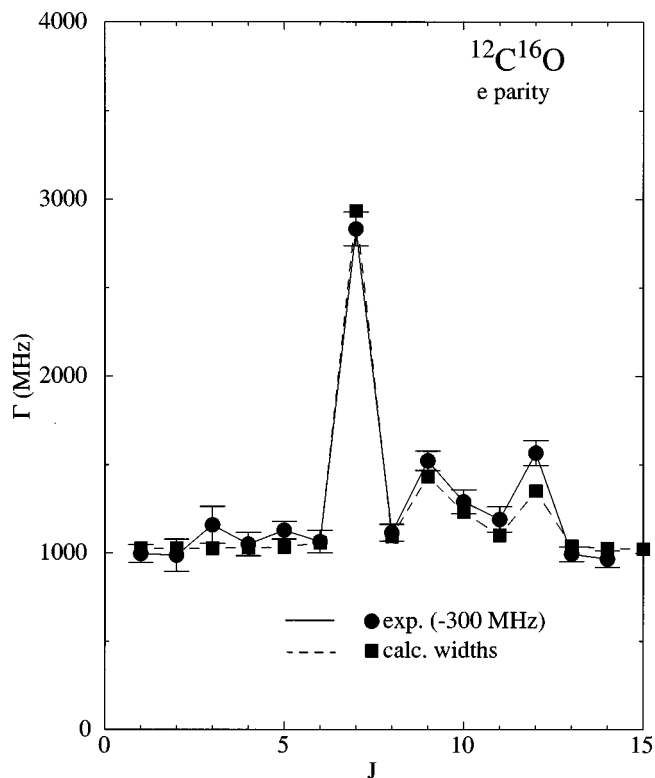


FIG. 11. Natural widths of the (e) parity resonances of the $E^1\Pi$, $v=1$ state of $^{12}\text{C}^{16}\text{O}$ as a function of J . The instrument width is deconvoluted from the observed widths by subtracting 300 MHz.

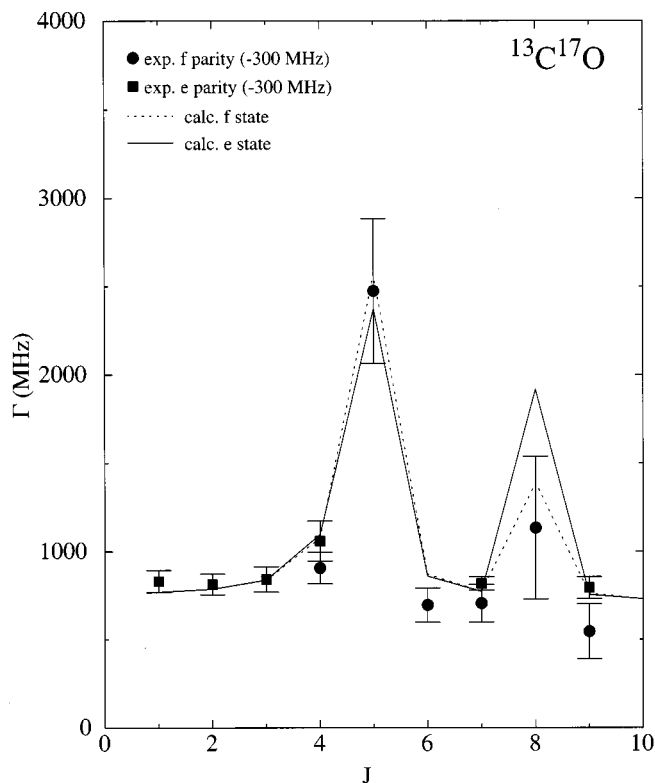


FIG. 12. Natural widths of the (*e*) and (*f*) parity resonances of the $E^1\Pi$, $v=1$ state of $^{13}\text{C}^{17}\text{O}$ as a function of J .

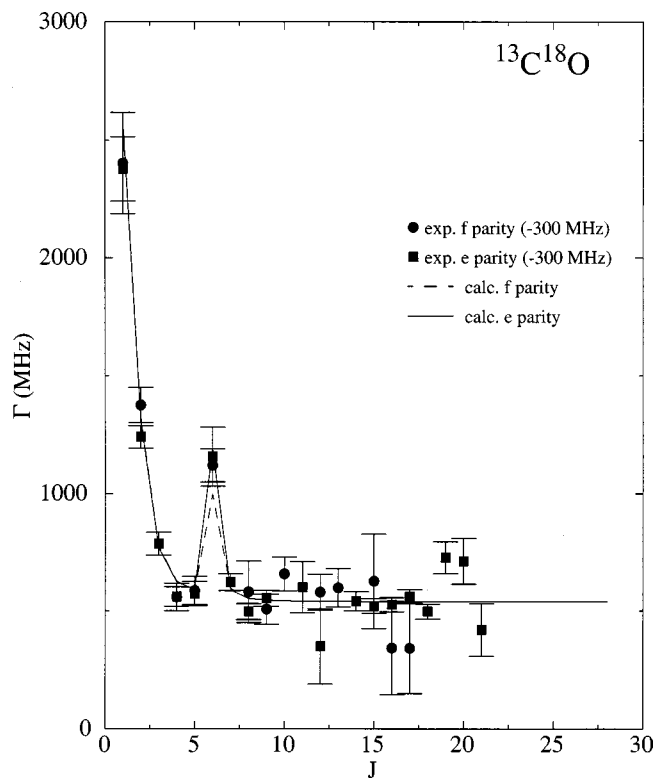


FIG. 13. Natural widths of the (*e*) and (*f*) parity resonances of the $E^1\Pi$, $v=1$ state of $^{13}\text{C}^{18}\text{O}$ as a function of J .

For three different isotopomers ($^{12}\text{C}^{16}\text{O}$, $^{13}\text{C}^{17}\text{O}$, and $^{13}\text{C}^{18}\text{O}$) the line broadening effects are explicitly shown in Figs. 11–13. Figure 11 displays the linewidths of the (*e*) parity components for $^{12}\text{C}^{16}\text{O}$ as a function of J ; in fact the natural line broadening Γ , due to a reduced lifetime as a result of predissociation, is deconvoluted from the observed width by subtracting the value for the instrument width of 300 MHz. The interaction at $J=7$ is clearly observable, while also $J=9$ and $J=12$ have increased widths. These J values correspond to the crossing points of $E^1\Pi$, $v=1$ with $k^3\Pi$, $v=6$ (see Fig. 9). In Fig. 12 a similar picture is shown for the natural line broadening parameters pertaining to both the (*e*) and (*f*) components of the $^{13}\text{C}^{17}\text{O}$ isotopomer. Resonances at $J=5$ and $J=8$ are in accordance with the findings of the spectral analysis and the crossing points in Fig. 9. In Fig. 13 the broadening parameters for the $^{13}\text{C}^{18}\text{O}$ isotopomer are displayed with resonances at $J=1$ and $J=6$.

It is important to note that the lines outside the regions of interaction with the $k^3\Pi$, $v=6$ state are intrinsically broadened as well; the interaction with the triplet state causes additional accidental predissociation. The data on line broadening, also for the other three isotopomers not explicitly shown, are included in an analysis similar to the one previously used for the lower resolution data.²² A quantitative analysis of the predissociation rates pertaining to each rotational quantum level entails diagonalization of the complex matrix:

$$\begin{bmatrix} E_E^{e,f}(J) - i\frac{\Gamma_E}{2} & 0 & H_{E,k} & 0 \\ 0 & k_{11}(J) - i\frac{\Gamma_k}{2} & k_{12}(J) & k_{13}(J) \\ H_{E,k} & k_{21}(J) & k_{22}(J) - i\frac{\Gamma_k}{2} & k_{23}(J) \\ 0 & k_{31}(J) & k_{32}(J) & k_{33}^{e,f}(J) - i\frac{\Gamma_k}{2} \end{bmatrix},$$

where the real part is similar to that of the spectroscopic analysis of the line shifts caused by the interaction. This part is kept fixed now for the computation of the predissociation rates by invoking the molecular constants as listed in Table VII. A decay rate Γ_k is defined for the perturbing $k^3\Pi$, $v=6$ state and Γ_E for the decay rate of $E^1\Pi$, $v=1$; good convergence in the procedures was found when the values for Γ_E and Γ_k were taken independent of (*e*)/(*f*) parity. The entire analysis is performed for each isotopomer independently. So an assumption is made that the predissociation effects on both states are caused by a homogeneous or J -independent interaction with continuum states. Values for Γ_E and Γ_k are optimized by comparing observed and calculated widths Γ_{obs} for all lines recorded; resulting values are listed in units of cm^{-1} in Table VIII. The uncertainties in the linewidths are estimated from the data sets and include statistical uncertainty as well as a systematic uncertainty related to the deconvolution procedure. For the $^{12}\text{C}^{17}\text{O}$ isotopomer

the information is too scarce to derive a value for Γ_k . As is shown in Fig. 2, for the $^{13}\text{C}^{16}\text{O}$ species the two interacting partners of the (e) parity components were both observed with their respective natural line broadening of 4.0 GHz for $^R R(6)$ and 3.6 GHz for $R(6)$. As the trace of the matrix is constant the sum of the linewidths of the two perturbed levels (7.6 GHz), equals the sum of Γ_E and Γ_k , and can hence be determined with high accuracy.

IV. DISCUSSION AND CONCLUSION

The $E-X(1,0)$ band has been reinvestigated in a high resolution 1VUV+1UV resonance enhanced two-photon ionization study using a Fourier-transform limited laser tunable near 105 nm. By the method of calibration with respect to an accurate wavelength standard the transition frequencies of the CO resonances could be determined with an absolute accuracy of 0.003 cm^{-1} . The data, including the energy levels that are perturbed up to 1.5 cm^{-1} , can be represented to this level of accuracy by a model involving a spin-orbit interaction between the $E^1\Pi$, $v=1$ and $k^3\Pi$, $v=6$ states. It is for the first time that rotational lines probing both (e) and (f) parity components are fully resolved and that line broadening parameters, associated with predissociation, are determined for each rotational quantum state. The previously obtained quantitative information on the phenomenon of accidental predissociation in the $E^1\Pi$, $v=1$ state, by Baker *et al.*¹³ and by our group,²² was indirect and less accurate. The nature of the accidental perturbation causing both shifts and line broadening was discussed previously. The $k^3\Pi$ and $E^1\Pi$ states differ by more than one orbital, but the spin-orbit-interaction between k and E states is nevertheless made possible by configuration interaction,¹⁵ the details of which are not fully understood so far.

Both the $E^1\Pi$, $v=1$ state and the $k^3\Pi$, $v=6$ state undergo overall predissociation, resulting from coupling to repulsive states; for this reason independent parameters Γ_E and Γ_k are determined in the experiment. It was assumed that the interaction of the $E^1\Pi$ and $k^3\Pi$ states with the continua gives rise to a J -independent interaction with continuum states. For the $E^1\Pi$, $v=1$ state this is certainly a valid assumption in view of the results as displayed in Figs. 11–13. For the $k^3\Pi$, $v=6$ state the situation would be less clear if only the results on a single isotopomer are considered; then the interaction is only at a few rotational lines. But if the data on all six isotopomers are included, with perturbations at almost all rotational levels, a consistent analysis can only be performed when the interaction between the $k^3\Pi$ state and

the perturbing continua is taken as J independent as well. The accidental predissociations in the $E^1\Pi$, $v=1$ state can be understood from the mixing with shorter lived triplet character; also quantitatively they can be fully reproduced by invoking a single J -independent coupling parameter $H_{E,k}$, which is nearly constant (within 0.01 cm^{-1}) over the six isotopomers at a value of 1.88 cm^{-1} .

The accidental predissociation, associated with the coupling between $E^1\Pi$, $v=1$ and $k^3\Pi$, $v=6$, is now fully described at a quantitative level for the six natural isotopomers of CO. The origin of the overall predissociation of each of the two states is less well understood. *Ab initio* quantum chemical calculations on the excited state potentials of CO, including the dissociative ones, have been performed by O'Neil and Schaefer¹⁸ and more recently by Hiyama *et al.*^{37,38} Two repulsive singlet states are clearly identified in the calculations, one of $^1\Sigma^+$ and one of $^1\Pi$ symmetry. The $^1\Sigma^+$ state even supports some bound levels at lower excitation energies and at large bond lengths; these levels were observed by Wolk and Rich,³⁹ who termed this state as $D'^1\Sigma^+$. This state crosses the higher lying Rydberg states and is responsible for predissociation of a number of states.⁴⁰ The J -dependent predissociation observed in the (e)^{40,41} parity components of the $L^1\Pi$, $v=0$ state, which is a state with a $4p\pi$ Rydberg orbital, is attributed to interaction with the repulsive part of $D'^1\Sigma^+$. For the (e) components an exact $J(J+1)$ functionality is observed. The predissociation of the (f) parity components of the $L^1\Pi$, $v=0$ state is much weaker and independent of J ^{28,41} and must be attributed to a different origin. These dependencies are the typical signature of a heterogeneous interaction between a bound state of $^1\Pi$ symmetry with a repulsive state of $^1\Sigma^+$ symmetry. Similar parity and rotational-state-dependent predissociation behavior, caused by the repulsive wall of the $D'^1\Sigma^+$ state, is observed in the $(3s\sigma)W^1\Pi$, $v=0$ state of CO.⁴⁰

The $E^1\Pi$ state has a $3p\pi$ Rydberg orbital, comparable to the $4p\pi$ orbital in the $L^1\Pi$, $v=0$ state, but here the predissociation rate is found to be independent of J (except for the accidental predissociation effects). The latter effect indicates a homogeneous coupling with a continuum of the same symmetry; hence we postulate that the E state is predissociated by the dissociative $^1\Pi$ state. Possibly the continuum of the bound $A^1\Pi$ state plays a role as well. After an *ab initio* calculation, Hiyama *et al.*³⁸ shifted the absolute energy of the repulsive $^1\Pi$ potential somewhat, based on a comparison with experimental findings of Komatsu *et al.*⁴² The dissociative $^1\Pi$ state indeed crosses the E -state potential; further calculations on the crossing between these states may establish the predissociation rates and values for Γ_E , including their isotope dependence, as found in the present study. These calculations should also reproduce the larger rate of predissociation in the $E^1\Pi$, $v=2$ state and the smaller rate for $E^1\Pi$, $v=0$.² Ebata and co-workers⁴³ have recently shown that the situation is even more complicated in observing that predissociation of singlet states via the triplet channel plays a role as well.

O'Neil and Schaefer¹⁸ have also calculated potential curves of $^3\Pi$ states. Their $^3\Pi(\text{II})$ state can be assigned as the $k^3\Pi$ state, while a $^3\Pi(\text{III})$ state is dissociative and gives rise

TABLE VIII. Natural line broadening coefficients Γ for the $E^1\Pi$, $v=1$ and $k^3\Pi$, $v=6$ states for the various isotopomers. Values are in cm^{-1} . Values given in parentheses signify the uncertainty in the last digits.

	Γ_E	Γ_k
$^{12}\text{C}^{16}\text{O}$	0.034 (3)	0.335 (10)
$^{12}\text{C}^{17}\text{O}$	0.024 (4)	
$^{12}\text{C}^{18}\text{O}$	0.024 (3)	0.28 (1)
$^{13}\text{C}^{16}\text{O}$	0.027 (3)	0.23 (1)
$^{13}\text{C}^{17}\text{O}$	0.024 (4)	0.20 (2)
$^{13}\text{C}^{18}\text{O}$	0.018 (3)	0.145 (5)

to an anticrossing in the adiabatic picture. It is feasible that predissociation of the $k^3\Pi$ state is an effect of tunneling through the potential barrier, formed by the two interacting $^3\Pi$ states. This might explain the isotopic dependence of the predissociation rates Γ_k . The tunneling rate for the heavier isotopomers is lower because of the higher mass and the lower energy in the potential well.

The line broadening parameters Γ can be related to excited state lifetimes τ via

$$\tau = \frac{1}{2\pi\Gamma c},$$

when Γ given in cm^{-1} and c the speed of light in cm/s . When the accidental predissociation effects are neglected and the values for Γ_E are taken as representing the lifetimes of the $E^1\Pi$, $v=1$ state then values for the excited state lifetime can be deduced: $\tau(^{12}\text{C}^{16}\text{O}) = 160 \pm 15$ ps, $\tau(^{13}\text{C}^{16}\text{O}) = 200 \pm 25$ ps, and $\tau(^{13}\text{C}^{18}\text{O}) = 300 \pm 50$ ps. These values can be compared with previously obtained values²³ from time-domain measurements using picosecond lasers in a pump-probe scheme, resulting in: $\tau(^{12}\text{C}^{16}\text{O}) = 118 \pm 20$ ps, $\tau(^{13}\text{C}^{16}\text{O}) = 198 \pm 25$ ps, and $\tau(^{13}\text{C}^{18}\text{O}) = 270 \pm 45$ ps. For $^{13}\text{C}^{16}\text{O}$ and $^{13}\text{C}^{18}\text{O}$ we find perfect agreement, while for the main isotopomer there is some discrepancy, although the values do match within 2σ uncertainty. It should be realized further that in the time-domain measurements no distinction was made between rotational levels and that probably the lowest eight rotational states were populated in the effusive molecular beam. In $^{13}\text{C}^{18}\text{O}$ there is a resonance at the very lowest rotational levels, as presently found; these levels give only a minor contribution to the signal in the direct decay measurements.

As for the astrophysical implications the predissociation yield, i.e., the probability of dissociative decay upon photoexcitation, is of importance. The predissociation yield η_{pre} is given by

$$\eta_{\text{pre}} = 1 - A_{\text{rad}}\tau,$$

where τ is the lifetime and A_{rad} is the radiative decay rate, summed over all possible radiative decay channels. In a previous paper Cacciani *et al.*²³ calculated values for the predissociation yield for three isotopomers $^{12}\text{C}^{16}\text{O}$, $^{13}\text{C}^{16}\text{O}$, and $^{13}\text{C}^{18}\text{O}$, where for $^{13}\text{C}^{18}\text{O}$ a lower value was found, in accordance with the smaller value of Γ_E for this isotopomer. One result of the present study is that the actual predissociation rate, and therewith also the predissociation yield varies with rotational quantum number. Specifically for $^{13}\text{C}^{18}\text{O}$ there is an increased predissociation for $J=1$ and $J=2$ levels. For the low temperatures in interstellar media (ranging from 3 to 50 K) the effective predissociation yield for $^{13}\text{C}^{18}\text{O}$ is much higher than calculated from Γ_E , due to the accidental resonance. In this laser spectroscopic study we will not elaborate further on the astrophysical implications. Suffice it to mention that the predissociation yields can be calculated for each quantum state of each of the six isotopomers, from the molecular parameters presented here.

ACKNOWLEDGMENTS

Financial support from the Foundation for Fundamental Research on Matter (FOM) is gratefully acknowledged. P.C. acknowledges support from the NWO/CNRS collaboration program.

- ¹C. Letzelter, M. Eidelsberg, F. Rostas, J. Breton, and B. Thieblemont, *Chem. Phys.* **114**, 273 (1987).
- ²M. Eidelsberg and F. Rostas, *Astron. Astrophys.* **235**, 472 (1990).
- ³E. F. van Dishoeck and J. H. Black, *Astrophys. J.* **334**, 771 (1988).
- ⁴J. J. Hopfield and R. T. Birge, *Phys. Rev.* **29**, 922 (1927).
- ⁵S. G. Tilford, J. T. Vanderslice, and P. G. Wilkinson, *Can. J. Phys.* **43**, 430 (1965).
- ⁶S. Ogawa and M. Ogawa, *J. Mol. Spectrosc.* **49**, 454 (1974).
- ⁷J. D. Simmons and S. G. Tilford, *J. Mol. Spectrosc.* **49**, 167 (1974).
- ⁸C. Amiot, J.-Y. Roncin, and J. Vergès, *J. Phys. B* **19**, L19 (1986).
- ⁹R. Kepa, *J. Mol. Spectrosc.* **132**, 545 (1988).
- ¹⁰G. Stark, P. L. Smith, K. Ito, and K. Yoshino, *Astrophys. J.* **395**, 705 (1992).
- ¹¹P. Klopotek and C. R. Vidal, *J. Opt. Soc. Am. B* **2**, 869 (1985).
- ¹²M. Hines, H. A. Michelsen, and R. N. Zare, *J. Chem. Phys.* **93**, 8557 (1990).
- ¹³J. Baker, J. L. Lemaire, S. Couris, A. Vient, D. Malmasson, and F. Rostas, *Chem. Phys.* **178**, 569 (1993).
- ¹⁴B. N. Wan and H. Langhof, *Z. Phys. D: At., Mol. Clusters* **21**, 245 (1991).
- ¹⁵J. Baker and F. Launay, *J. Mol. Spectrosc.* **165**, 75 (1994).
- ¹⁶J. Baker, *J. Mol. Spectrosc.* **167**, 323 (1994).
- ¹⁷J. Mazeau, C. Scherman, and G. Joyez, *J. Electron Spectrosc. Relat. Phenom.* **7**, 269 (1975).
- ¹⁸S. V. O'Neil and H. F. Schaefer III, *J. Chem. Phys.* **53**, 3994 (1970).
- ¹⁹A. Mellinger and C. R. Vidal, *J. Chem. Phys.* **101**, 104 (1994).
- ²⁰G. Berden, R. T. Jongma, D. van der Zande, and G. Meijer, *J. Chem. Phys.* **107**, 8303 (1997).
- ²¹I. Dabrowski, M. Vervloet, and D.-C. Wang, *Can. J. Phys.* **65**, 1171 (1987).
- ²²P. Cacciani, W. Hogervorst, and W. Ubachs, *J. Chem. Phys.* **102**, 8308 (1995).
- ²³P. Cacciani, W. Ubachs, P. C. Hinnen, C. Lyngå, A. L'Huillier, and C.-G. Wahlström, *Astrophys. J. Lett.* **499**, L223 (1998).
- ²⁴W. F. Chan, G. Cooper, and C. E. Brion, *Chem. Phys.* **170**, 123 (1993).
- ²⁵M. Ciocca, I. Kanik, and J. M. Ajello, *Phys. Rev. A* **55**, 3547 (1997).
- ²⁶K. Kirby and D. L. Cooper, *J. Chem. Phys.* **90**, 4895 (1989).
- ²⁷K. S. E. Eikema, W. Ubachs, W. Vassen, and W. Hogervorst, *Phys. Rev. A* **55**, 1866 (1997).
- ²⁸W. Ubachs, K. S. E. Eikema, W. Hogervorst, and P. C. Cacciani, *J. Opt. Soc. Am. B* **14**, 2469 (1997).
- ²⁹I. Velchev, R. van Dierendonck, W. Hogervorst, and W. Ubachs, *J. Mol. Spectrosc.* **187**, 21 (1998).
- ³⁰S. C. Xu, R. van Dierendonck, W. Hogervorst, and W. Ubachs, *J. Mol. Spectrosc.* (in press).
- ³¹C. Sansonetti, *J. Opt. Soc. Am. B* **14**, 1913 (1997).
- ³²I. Velchev, W. Hogervorst, and W. Ubachs, *J. Phys. B* **32**, L511 (1999).
- ³³G. Guelachvili, D. de Villeneuve, R. Farrenq, W. Urban, and J. Vergès, *J. Mol. Spectrosc.* **98**, 64 (1983).
- ³⁴R. W. Field, S. G. Tilford, R. A. Howard, and J. D. Simmons, *J. Mol. Spectrosc.* **44**, 347 (1972).
- ³⁵J. M. Brown, E. A. Colbourn, J. K. G. Watson, and F. D. Wayne, *J. Mol. Spectrosc.* **74**, 294 (1979).
- ³⁶C. Amiot, E. M. Azaroual, P. Luc, and R. Vetter, *J. Chem. Phys.* **102**, 4375 (1995).
- ³⁷M. Hiyama and H. Nakamura, *Chem. Phys. Lett.* **248**, 316 (1996).
- ³⁸M. Hiyama, N. Kosugi, and H. Nakamura, *J. Chem. Phys.* **107**, 9370 (1997).
- ³⁹G. L. Wolk and J. W. Rich, *J. Chem. Phys.* **79**, 12 (1983).
- ⁴⁰K. S. E. Eikema, W. Hogervorst, and W. Ubachs, *Chem. Phys. Lett.* **181**, 217 (1994).
- ⁴¹M. Drabbe, J. Heinze, J. J. ter Meulen, and W. L. Meerts, *J. Chem. Phys.* **99**, 5701 (1993).
- ⁴²M. Komatsu, T. Ebata, and N. Mikami, *J. Chem. Phys.* **99**, 9350 (1993).
- ⁴³A. Okazaki, T. Ebata, T. Sutani, and N. Mikami, *J. Chem. Phys.* **108**, 1765 (1998).